DOI: 10.1007/s43153-020-00039-5

Brazilian Journal of Chemical Engineering
https://doi.org/10.1007/s43153-020-00039-5

ORIGINAL PAPER

An enhanced weighted essentially non-oscillatory high order scheme for explosion modelling

Elmo de Sena Ferreira Jr[1] · Sávio Souza Venâncio Vianna[1]

Received: 29 February 2020 / Revised: 24 June 2020 / Accepted: 27 June 2020

Abstract

Physical explosion causes large damages in the process industry and quite often escalates to chemical explosions. The shock waves generated by such events are challenging to model and they must be numerically captured without spurious oscillations in order to make an accurate estimative of the accidental effects. In this context, this paper investigates how a new high order numerical scheme models the physical explosion. We have considered a confined explosion in a spherical vessel and blast load throughout pipelines as the framework to investigate the performance of the numerical scheme. The developed numerical approach considers the effect of less smooth substencils when there is a discontinuity inside the stencil based on the local Mach number what avoids oscillations and instability. The numerical solution of the fundamental equations is coupled with the Modified Colebrook-White formulation in order to consider the blast load through the pipeline. Shock waves from experimental data and analytical model are used to validate the proposed model. The research provides an efficient method for prediction of blast loads from spherical vessels rupture to an open atmosphere and in pipelines.

Keywords Weighted essentially non oscillatory scheme · Physical explosion · Process safety

Introduction

Explosion in the process industry is among the most severe accidents leading to significant losses and contributing to the risk level of chemical process facilities. The accidental explosions can be split into chemical explosion and physical explosion. In accordance with Abbasi and Abbasi (2007), chemical explosion may be based on deflagration or detonation depending on the speed of the propagation of the flame front. On the other hand, physical explosions are classified as compressed gas/vapour explosion (CG/CE), boiling liquid expanding vapor explosion (BLEVE) and rapid phase transition (RPT) explosion. Several accidents due to physical and/or chemical explosions are described in the literature (Lewis 1980; Khan and Abbasi 1999; FI 1999). In 2018, the Petrobras refinery at Paulinia (Replan—Sao Paulo—Brazil) experienced a physical explosion followed by chemical explosion at the storage tank of acid waters. Significant damage to equipment was observed and it halted the production.

The understanding of explosion phenomenon and the associated impact in the industry helps to enhance safety in various industrial sites. Experiments concerning explosions, however, are costly and potentially dangerous (Oliveira et al. 2019). Alternatively, numerical simulations can help to shed light on the comprehension of various aspects of the phenomenon. Most of the numerical approaches concerning the modelling of accidental releases that can potentially lead to explosion rely on the finite volume method (FVM) in which the derivatives are addressed by mean of first and second order discretisation schemes (Fiates and Vianna 2016; Ferreira and Vianna 2016; Ferreira et al. 2019). It turns out that additional difficulties arise when discontinuities and shock waves are present in the phenomena. In most cases, very refined meshes are necessary and the computational cost may skyrocket. Advantage and disadvantages concerning numerical schemes applied in explosion analysis have been extensively discussed (Leak 2002).

It has been suggested that high-order numerical schemes emerge as a potential alternative for improvement of explosion studies. In the context of high-order schemes, WENO (weighted essentially non oscillatory) schemes have demonstrated to be robust and efficient (Borges et al. 2008; Hu et al. 2016; Acker et al. 2016) and recent papers indicate

✉ Sávio Souza Venâncio Vianna
svianna@unicamp.br

[1] University of Campinas, Campinas, Brazil

Published online: 08 July 2020

that numerical modelling of explosions are under continuous development relying on WENO approaches (Wang et al. 2013, 2015; Xu et al. 2018). Combined adaptive mesh refinement (AMR) to WENO scheme has been applied in the investigation of denotation (Wang et al. 2015). More recently, researchers (Xu et al. 2018) proposed a new WENO scheme in order to evaluate the blast wave in a partially confined chamber and a simplified analytical model was developed to predict quasi-static overpressure. Other classes of high-order numerical scheme for explosion study have been proposed [(namely modified Harten's (Total Variation Diminishing) TVD scheme] in order to capture the main regions of the shock wave of physical explosion; main shock, second shock and the contact discontinuity region (Liu et al. 1999). Such scheme comes from the coupling between artificial compression method (ACM) and Harten's TVD scheme. Although the Harten's TVD scheme may smear the contact discontinuity, the idea of Liu et al. (1999) was to include ACM method restricted to the immediate region of the contact discontinuity, increasing the resolution of contact discontinuity.

However, all approaches concerning WENO schemes rely on the mesh size as the tuning parameter for the contribution of less smooth stencils when there is a discontinuity. The current methods do not consider any physical insight when enhancing the contribution from less smooth stencils. In the current work we propose the modification of the parameter tuning the size of the increment of the weight concerning the less smooth regions of the computational mesh based on the local Mach number.

We have also coupled the proposed WENO-SV scheme with the Pressure Vessel Failure model (PVF model) (Crowl and Louvar 2002) to study physical explosion leading to the PVF/WENO-SV model. The PVF model calculates the pressure required for the vessel rupture providing appropriate initial condition while WENO-SV captured the shock waves. The explosion is modelled via the Euler equation considering a spherical source term. The WENO-SV scheme solves the Euler conservative equations considering the method of characteristics. Time advancement is achieved using the third-order Strong Stability Preserving Runge-Kutta algorithm—SSP-RK(3,3). The Lax-Friedrich flux splitting is employed for upwind correction of the flow. In order to compute blast waves throughout pipelines, WENO-SV scheme is combined with Modified Colebrook-White formulation (lead to WENO-SV/pipeline model) which is responsible for modelling of the loss of energy in the pipe.

The results are compared with experimental and analytical data. Good agreement is observed for both models. PVF/WENO-SV model captured the features of the shock wave after the glass explosion and WENO-SV/pipeline model computed blast waves travelling throughout the pipeline.

The paper is organised as follows. In the next section the WENO-SV scheme is introduced and the procedure to deal with spherical modelling is discussed. The following section addresses the coupling of the pipeline model. The results are discussed in Sect. 4. In the last section, the conclusions are drawn.

Numerical method

Governing equations

The one-dimensional Euler equation of motion for radially symmetric flow is usually written in the following form,

$$\frac{\partial \mathbf{Q}}{\partial t} + \frac{\partial \mathbf{f}(\mathbf{Q})}{\partial r} = \mathbf{S}(Q), \tag{1}$$

where

$$\mathbf{Q} = \begin{bmatrix} \rho \\ \rho u \\ E \end{bmatrix}, \mathbf{f}(Q) = \begin{bmatrix} \rho u \\ \rho u^2 + p \\ u(E+p) \end{bmatrix}, \qquad \mathbf{S}(Q) = -\frac{\theta}{r}\begin{bmatrix} \rho u \\ \rho u^2 \\ u(E+p) \end{bmatrix} \tag{2}$$

the vectors of the conserved variables and fluxes are $\mathbf{Q}$ and $\mathbf{f(Q)}$, respectively. The independent variables are time (t) and the radial distance from the centre of the explosion (r). The dependent variables are density (ρ), radial velocity (u), pressure (p) and total energy per unit volume (E). $\mathbf{S(Q)}$ is the source term. In Eq. (2), $\theta = 1$ and $\theta = 2$ are variables accounting for cylindrical and spherical shapes considered in the explosion modelling, respectively.

For perfect gases, the following formulation for the equation of state was adopted

$$p = (\gamma - 1)\left(E - \frac{1}{2}\rho u^2\right) \tag{3}$$

where γ is the specific heat ratio.

WENO numerical scheme

Fundamentals

In order to introduce the new discretisation scheme, we initially describe the generic one-dimensional formulation of fifth-order WENO scheme when applied to hyperbolic conservation laws in the form presented in Eq. (1) with no source term for the sake of simplicity. Namely, the flux derivative $\frac{\partial f(Q)}{\partial r}$ (written as $f(Q)_r$) is approximated by the conservative flux difference as follows

$$f(Q)_r \mid_{r=r_i} = \frac{1}{\Delta r}\left(\hat{f}_{i+1/2} - \hat{f}_{i-1/2}\right) \tag{4}$$

where the numerical flux $\hat{f}_{i+1/2}$ depends on the five grid point values, $f(Q_j)$, $j = i-2, \ldots, i+2$ for the positive wave. This numerical flux $\hat{f}_{i+1/2}$ may be written as a convex combination of three numerical fluxes (third order) as follows

$$\hat{f}_{i+1/2} = \omega_0 f^{(0)} + \omega_1 f^{(1)} + \omega_2 f^{(2)} \tag{5}$$

where $f^{(0)}$, $f^{(1)}$, $f^{(2)}$ are the fluxes based on three distinct sub-stencils comprising three points each set as

$$\begin{cases} f^{(0)} = \frac{1}{3}f_{i-2} - \frac{7}{6}f_{i-1} + \frac{11}{6}f_i \\ f^{(1)} = -\frac{1}{6}f_{i-1} + \frac{5}{6}f_i + \frac{1}{3}f_{i+1} \\ f^{(2)} = \frac{1}{3}f_i + \frac{5}{6}f_{i+1} - \frac{1}{6}f_{i+2} \end{cases} \tag{6}$$

The combination coefficients depend on the smoothness indicator ω_k measuring the smoothness of the solution in each stencil (Jiang and Shu 1996), where

$$\omega_k = \frac{\alpha_k}{\alpha_0 + \alpha_1 + \alpha_2}, \quad k = 0, 1, 2. \tag{7}$$

The original formulation of the normalised nonlinear weights embedded in the WENO-Z+ scheme (Acker et al. 2016) is implicitly based on the mesh size through the tune λ^{z+} parameter in the second term of Eq. (8).

$$\alpha_k^{z+} = d_k\left[1 + \left(\frac{\tau}{\beta_k + \epsilon}\right)^p + \zeta^{z+}\right]. \tag{8}$$

where

$$\zeta^{z+} = \lambda^{z+}\left(\frac{\beta_k + \epsilon}{\tau + \epsilon}\right) \quad \tau = \mid \beta_2 - \beta_0 \mid . \tag{9}$$

$$d_0 = \frac{1}{10}, d_1 = \frac{6}{10}, d_2 = \frac{3}{10} \tag{10}$$

and ϵ is a positive real number introduced to avoid singularity (usually $\epsilon = 10^{-16}$) and $p = 2$. The smooth indicator is

$$\begin{aligned}\beta_0 = &\frac{1}{4}\left(f_{i-2} - 4f_{i-1} + 3f_i\right)^2 \\ &+ \frac{13}{12}\left(f_{i-2} - 2f_{i-1} + f_i\right)^2\end{aligned} \tag{11}$$

$$\begin{aligned}\beta_1 = &\frac{1}{4}\left(-f_{i-1} + f_{i+1}\right)^2 \\ &+ \frac{13}{12}\left(f_{i-1} - 2f_i + f_{i+1}\right)^2\end{aligned} \tag{12}$$

$$\begin{aligned}\beta_2 = &\frac{1}{4}\left(-3f_i + 4f_{i+1} - f_{i+2}\right)^2 \\ &+ \frac{13}{12}\left(f_i - 2fi + 1 + f_{i+2}\right)^2\end{aligned} \tag{13}$$

WENO-SV formulation

The new formulation is based on the classification of partial differential equations as far as the inviscid flows are concerned. Therefore, considering the compressibility effects, is reasonable to take into account the magnitude of the Mach number. For Mach numbers above unity, the pressure influence at events upstream is not feasible leading to a zone of influence that turns out to be the main aspect of hyperbolic behaviour. Such flows are entitled to comprise wave discontinuities dividing regions of subsonic flows (elliptic behaviour) and regions of supersonic flows (hyperbolic behaviour) in which the precise location is not easy to know in advance.

Motivated by the discussion above, it seems sensible to replace the tuning parameter λ^{z+} from Eq. (8) by a physical parameter. It is important to bear in mind that extra contribution from WENO-Z+ scheme allows for the increasing of the contribution of the weights of less smooth substencils. Such contribution is solely based on $\lambda^{z+} \sim \Delta x^{2/3}$ in previous formulations, as WENO-Z+ (Acker et al. 2016).

Therefore, based on the location of the shock wave, it is suggested to modify λ^{z+} based on the underlying physics embedded in the local Mach number. Hence, the following formulation is proposed:

$$\lambda^{SV} = \sqrt{M} \tag{14}$$

where M is the local Mach number. Substitution of Eq. (14) in Eq. (8) leads to

$$\alpha_k = d_k\left[1 + \left(\frac{\tau}{\beta_k + \epsilon}\right)^p + \zeta^{SV}\right] \tag{15}$$

where

$$\zeta^{SV} = \lambda^{SV}\left(\frac{\beta_k + \epsilon}{\tau + \epsilon}\right) \quad \tau = \mid \beta_2 - \beta_0 \mid . \tag{16}$$

The λ^{SV} was determined based on the stability of standard test cases. The λ^{SV} parameter was investigated for $M^{0.5}$, $M^{0.25}$ and M, where M is the local Mach number. Numerical observations have shown that all λ^{SV} parameters are potential candidates to the new parameter. We therefore selected $\lambda^{SV} = M^{0.5}$.

Algorithm 1: Source term implementation.

```
for i ← 1 to ni do
    s(1,i) = [-theta(i)/r(i)]*flux(1,i) ;
    s(2,i) = [-theta(i)/r(i)]*(flux(2,i) - p(i)) ;
    s(3,i) = [-theta(i)/r(i)]*flux(3,i) ;
end
```

Algorithm 2: flux discretisation plus source term.

```
for i ← 1 to ni do
    L(1,i) = (flux(1,i+1)-flux(1,i))/dx + (s(1,i)+s(1,i+1))*0.5 ;
    L(2,i) = (flux(2,i+1)-flux(2,i))/dx + (s(2,i)+s(2,i+1))*0.5 ;
    L(3,i) = (flux(3,i+1)-flux(3,i))/dx + (s(3,i)+s(3,i+1))*0.5 ;
end
```

Source term treatment by WENO-SV scheme

In the current research two problems have been solved considering the source term: the physical explosion and Rayleigh-Taylor instability problem.

Since we were focused on physical explosion investigation, we consider Rayleigh-Taylor instability problem to verify the treatment of the source term. Similar analysis of the Rayleigh-Taylor instability problem can be found elsewhere (Borges et al. 2008; Hu et al. 2016).

The source term $S_{i+1/2}$ was calculated based on the reconstructed fluxes by the WENO-SV scheme. The source term for mass (ρu) and energy $(u(E+p))$, presented in Eq. (2), are exactly the same of the corresponding fluxes due to conserved variables. The momentum source term (ρu^2) is computed by means of the pressure (p) from the momentum flux (ρu^2+p). Therefore, since the fluxes are reconstructed for the left hand side of Eq. (2), so is the source term.

Details of the source term implementation, as it was coded, can be found in the algorithm 1 described below. The source terms for mass, momentum and energy are, $S(1, i)$, $S(2, i)$ and $S(3, i)$, respectively. The variables $flux(1, i)$, $flux(2, i)$ and $flux(3, i)$ are the WENO-SV reconstructed fluxes of mass, momentum and energy, respectively. The fluxes are coded as detailed by algorithm 2.

At this point is important to mention that it has been observed reduction of the order of accuracy. The degradation of the order of the accuracy is due to regions where the shock is present. As it is, it might well be that the information that travels through the shock may be lost. There have been attempts (Gottlieb et al. 2006) to overcome this matter using post processing techniques that are able to recover the order of accuracy up to the shock location. In the current formulation we are not considering it. Since we want to investigate how the model works it was important to avoid any technique that could mislead the main findings. Having said that, it is worthy exploring it in future publications.

Time marching method

The third-order SSP-RK(3,3) method is applied for the unsteady time integration as follows

$$\begin{cases} Q^{(1)} = Q^{(n)} + \Delta t L(Q^{(n)}) \\ Q^{(2)} = \frac{3}{4}Q^{(n)} + \frac{1}{4}Q^{(1)} + \frac{1}{4}\Delta t L(Q^{(1)}) \\ Q^{n+1} = \frac{1}{3}Q^{(n)} + \frac{1}{3}Q^{(2)} + \frac{2}{3}\Delta t L(Q^{(2)}) \end{cases} \tag{17}$$

The value for Δt is computed based on Courant-Friedrichs-Lewy (CFL) condition. The calculation for $L(Q)$ follows the same approach described in algorithm 2.

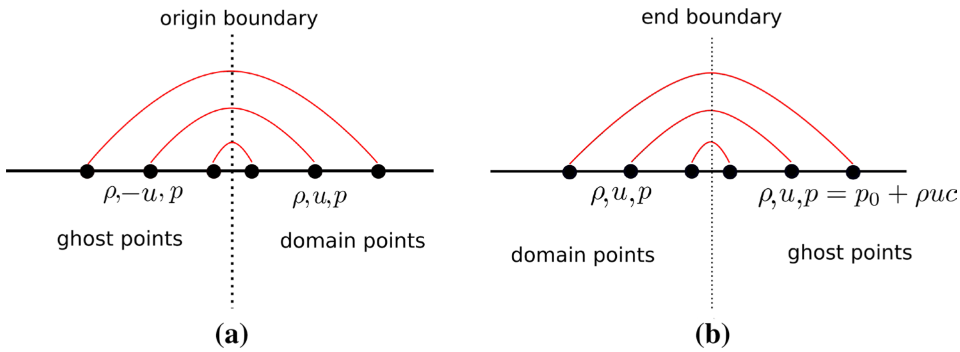

Fig. 1 Schematic of the symmetry boundary condition (**a**) and transmitting boundary condition (**b**)

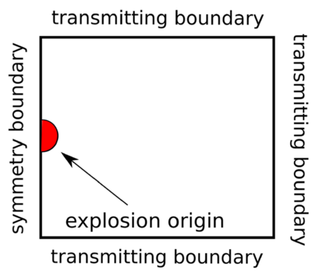

Fig. 2 Computational domain. The red semi-circle indicates the initial kernel of the explosion

Singularity and boundaries

The symmetry conditions for $\mathbf{Q}$ must be satisfied at $r = 0$ for axisymmetric problems. This issue is addressed by considering the following form for the conservation equation

$$\frac{\partial \mathbf{Q}}{\partial t} + \frac{\partial \mathbf{F}(\mathbf{Q})}{\partial r} = 0, \quad u = 0 \tag{18}$$

Ghost points have been employed to model the boundary conditions at the end close to the ignition source and to the far end of the computational domain. Symmetry condition was considered at the end where the kernel of the explosion is placed. Everywhere else, transmitting boundary conditions were applied.

Figure 1 shows the concept of symmetry and transmitting boundary condition at the left and right ends of the computational domain. Figure 2 shows the location of the boundary conditions.

The solver has been coded in Fortran 90. The simulations have been performed in a serial computer (I7 processor and 32 Gb RAM).

Verification of the new scheme

In this section, we investigate through numerical experiments the main implications of changing WENO-Z+ parameter, λ^{z+}, to WENO-SV parameter, λ^{sv}. We also call attention to the strengths and weaknesses of the WENO-Z+ scheme that motivated the new proposed numerical approach.

One of the major strengths of the WENO Z+ lies on the fact that the scheme places larger weights on the less smooth substencils instead of the critical points as suggested by previous WENO numerical formulations. This contribution is due to the fact that substencils containing critical points are smooth when coarse grids are considered. As a consequence, it leads to less dissipative results (Acker et al. 2016).

On the other hand, in the WENO Z+ formulation is well documented that the parameter λ^{z+} is based on guesses which are based on empirical tests. Therefore, it might be far from optimal and it deserves further investigation. In fact, the authors mention that the λ^{z+} parameter itself depends on the grid size and it would be of interest to remove this dependency (De Rezende Borges 2017).

The new parameter λ^{sv}

In order to investigate how the proposed λ^{sv} parameter behaves, we had followed the same methodology applied to WENO Z+ (Acker et al. 2016) where three distinct tuning parameters candidates were verified. We have considered two classical oscillatory wave problems due to Shu and Osher and Titarev-Toro.

At this point, it is worth mentioning that the developed method is focused on the problems where there are discontinuities. Hence, smooth regions where the local Mach

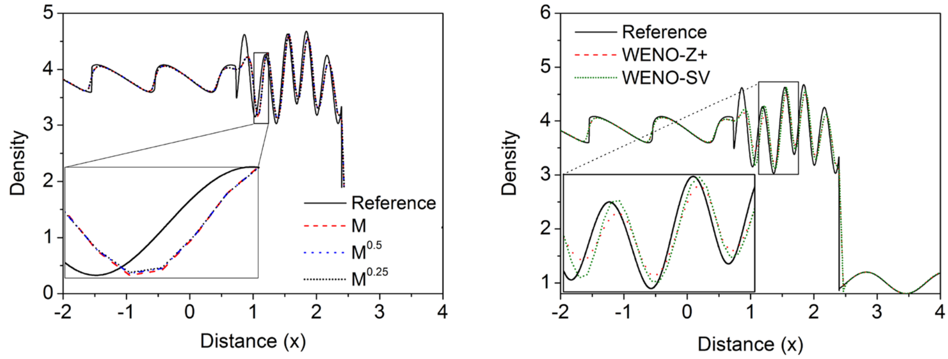

(a) (b)

Fig. 3 Density profile of the shock problem due to Shu and Osher considering the distinct λ^{sv} parameters (**a**). Comparison of the proposed method with the WENO-Z+ for the density profile along the x-line (**b**)

number is high are not considered in the current research. Having said, it might well be of interest in future work.

We next present the numerical findings for three λ^{sv} parameters based on the local Mach number (M, $M^{0.5}$ and $M^{0.25}$). The selection of the exponents is empirical.

Analysis of Figure 3a shows how the density varies along the $x - line$ for the parameters investigated considering the Shu-Osher problem. There seems to be no significant difference among the parameters considered when the numerical results are compared with the benchmark case (numerical solution using WENO-JS and 8000 grid points).

Figure 3b compares the new parameter (set as $M^{0.5}$) with the original WENO-Z+ formulation. It can be seen that WENO-SV performs better than WENO-Z+. The inner image in Fig. 3b provides evidence of the performance of the new approach.

Additionally, we show how the new approach compares with one of the pioneers schemes (WENO-JS), suggested by Jiang and Shu. Analysis of Fig. 4 shows that WENO-SV easily outperforms the classical WENO-JS.

Bearing in mind that Shu and Osher problem deals with Mach numbers above unity, we have considered another problem due to Titarev-Toro that addressed fairly lower Mach numbers (around 0.4) and an increased number of oscillations.

It is clear from Fig. 5 that the proposed method led to numerical results much closer to the benchmark findings. Figure 5a compares WENO-SV with WENO-JS and Fig. 5b compares WENO-SV with WENO-Z+. Analysis of Fig. 5a and b shows that WENO-SV captured the oscillations far better than WENO-JS and WENO-Z+.

Although WENO-SV seems to be handling the oscillations quite well, it is not clear how the scheme would behave for this class of problem should the Mach number be higher. It might be that the combination of the grid size and the

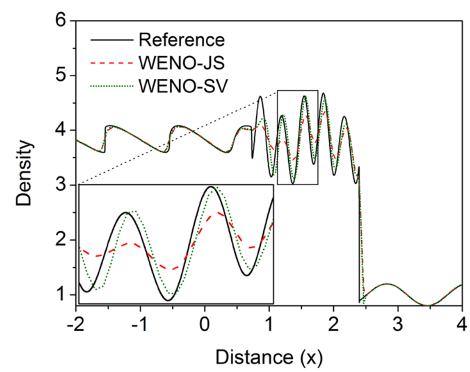

Fig. 4 Comparison of the performance of WENO-SV and WENO-JS for the Shu and Osher problem

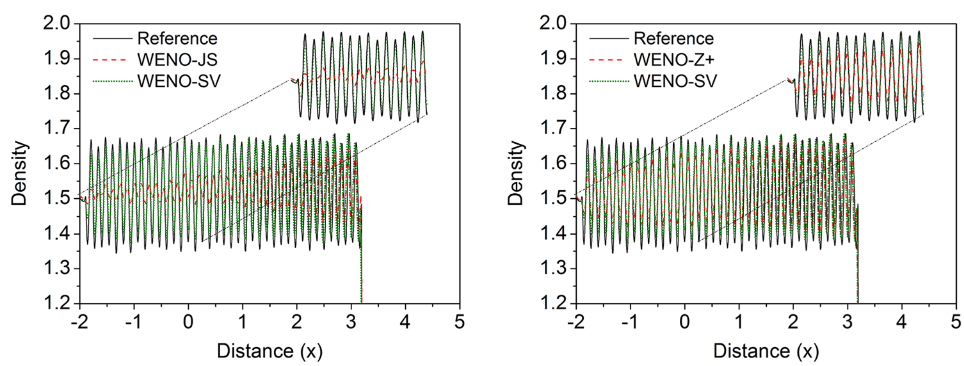

(a) (b)

Fig. 5 Density profile of the shock problem due to Shu and Osher considering the distinct λ^{sv} parameters (**a**). Comparison of the proposed method with the WENO-Z+ (**b**) for the density profile along the x-line

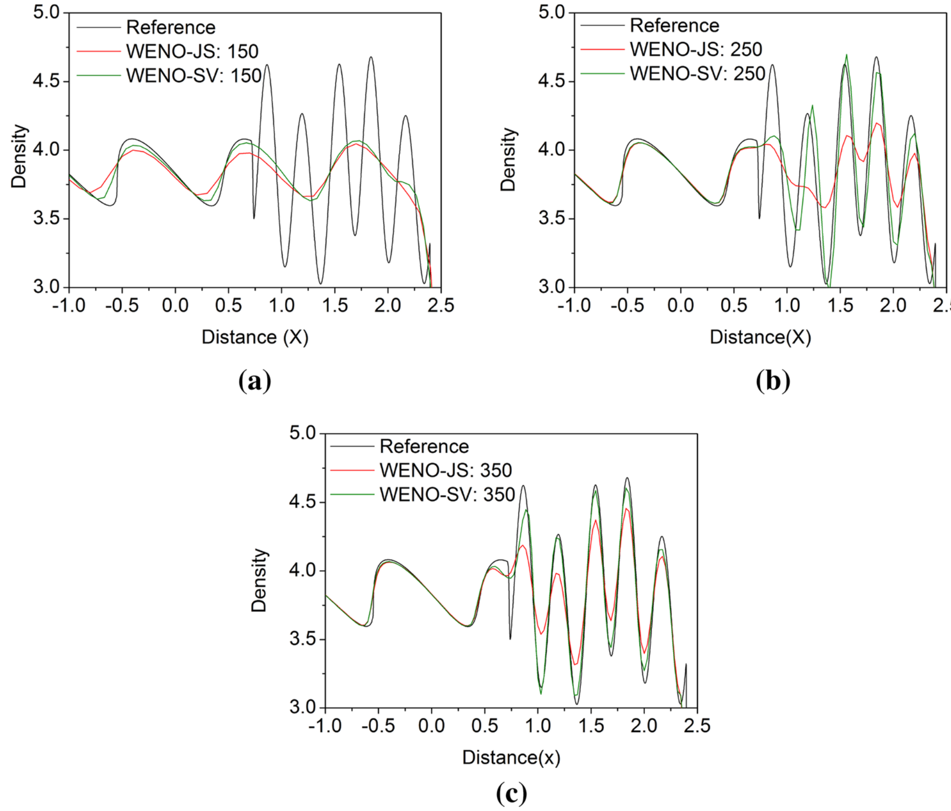

Fig. 6 Density profile of the shock problem due to Shu and Osher considering three mesh sizes. **a** Comparison of the proposed method with the WENO-JS for N = 150. **b** Comparison of the proposed method with the WENO-JS for N = 250. **c** Comparison of the proposed method with the WENO-JS for N = 350

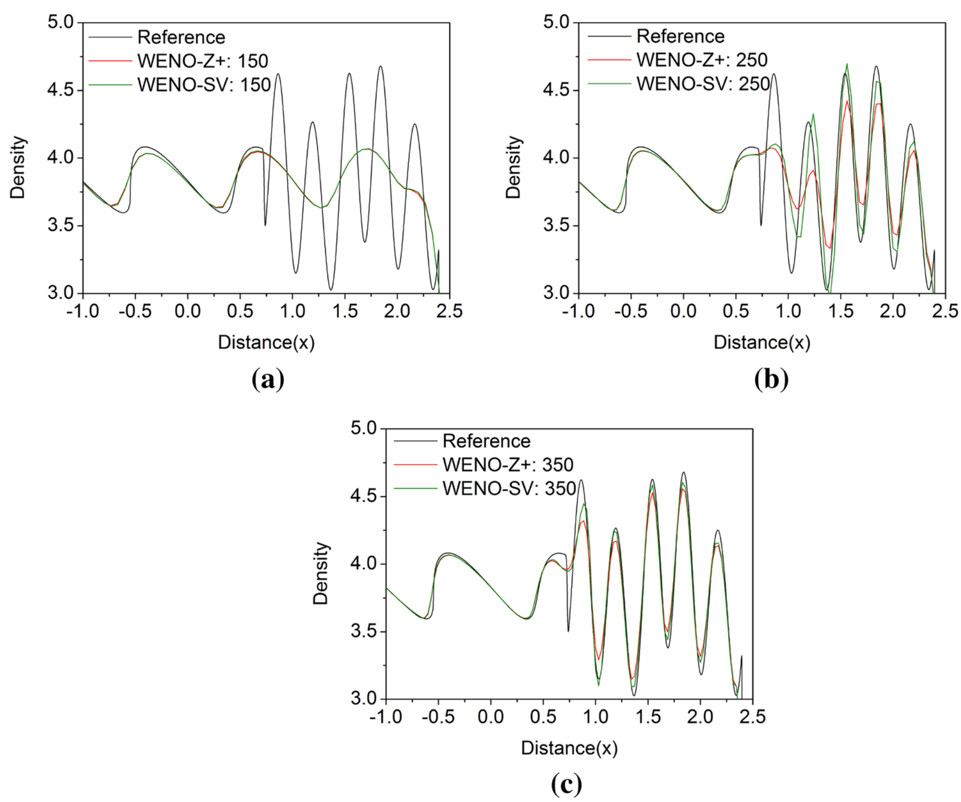

Fig. 7 Density profile of the shock problem due to Shu and Osher considering three mesh sizes. **a** Comparison of the proposed method with the WENO-Z+ for N = 150. **b** Comparison of the proposed method with the WENO-Z+ for N = 250. **c** Comparison of the proposed method with the WENO-Z+ for N = 350

Mach number would lead to a better way to address this matter. We are not exploring this route at the moment, but it certainly deserves a closer look in the near future.

Based on the discussion above, we have selected the $\lambda^{sv} = M^{0.5}$. In the next section the mesh refinement is addressed.

Mesh refinement analysis

The first set of mesh refinement was assessed considering the shock-entropy problem wave due to Shu and Osher. In order to verify how the method behaves for different mesh sizes (N = 150, N = 250 and N = 350 nodes), we show the initial density profile at $t = 1.8s$.

Figure 6 compares the density profile considering the three mesh sizes previously mentioned. It also compares the performance of WENO-SV with the performance of WENO-JS. The agreement with the reference solution is enhanced as the number of the grid points increase. Overall, WENO-SV was able to capture the oscillations much better than WENO-JS.

We also investigated how WENO-SV compares with WENO-Z+. The same approached adopted at the comparison with WENO-JS (please refer to Fig. 6) is applied here.

Analysis of Fig. 7 shows that WENO-SV captured details of the flow that WENO-Z+ was not able to capture. Analysis of Fig. 7b shows that even with a coarse mesh (N = 250), WENO-SV was able to follow the oscillations very close to the exact solution. WENO-Z+, on the other hand, struggled to mimic the oscillations. Considering the case in which N = 350 (Fig. 7c), WENO-Z+ improved the numerical solution. However, a closer look at Fig. 7c shows that the numerical results using WENO-SV are in better agreement with the reference solution than WENO-Z+.

The effect of weights on WENO-Z+ and WENO-SV

We first analyse the λ parameter as it has been coded in WENO-Z+ and WENO-SV, $\lambda^{z+} = \Delta x^{2/3}$ and $\lambda^{sv} = M^{0.5}$, respectively.

Both λ parameters are plotted in Fig. 8. Figure 8a shows WENO-SV λ on the vertical axis and WENO-Z+ λ on the horizontal axis for the shock entropy problem at $t = 1.8s$. The cases considered three grid sizes since the WENO-Z+ λ depends on Δx.

Analysis of Fig. 8a shows that as the grid size reduces the value of λ reduces since $\lambda \sim \Delta x$. However, for all grid sizes considered the λ parameter due to WENO-SV is far larger than the λ parameter due to WENO-Z+.

Further insight can be obtained by analysing the term ζ^{z+} and ζ^{sv} (the additional unnormalised nonlinear weights). As far as the shock-entropy is concerned, the term ζ^{SV} is greater than ζ^{z+} at some regions and slightly smaller at others, as shown in Fig. 8b.

The combined effect of the influence of λ and ζ can certainly be better understood when Eq. (15) is brought into the discussion. Therefore, the previous discussion recalls Eq. (15).

Overall it is clear that λ^{z+} is grid dependant while λ^{sv} is problem dependant. The former is closely related to the grid size and the latter is related to the physical nature of the problem.

Rayleigh-Taylor instability problem

Prior to moving on to the explosion modelling, we applied the proposed scheme to verify how the method computes the solution of a problem comprising complex flow features. Figure 9 shows the results for the 2D test case considering the Rayleigh-Taylor instability.

Analysis of Fig. 9 shows that WENO-SV is able to capture details of the flow features that were not computed by the WENO-JS and WENO-Z+. The latter scheme, however, provides a solution very similar to the one obtained when

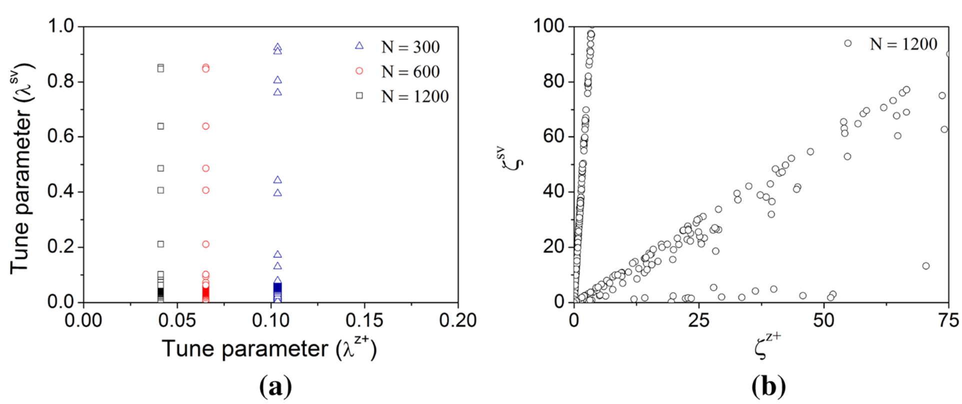

Fig. 8 WENO-Z+ parameter $\lambda^{z+} = \Delta x^{2/3}$ and WENO-SV parameter $\lambda^{sv} = M^{0.5}$ values is different grid sizes. **a**, **b** ζ parameter for WENO-SV and WENO-Z+. The Shock-entropy wave problem of Shu at time $t = 1.8s$ was considered in this analysi

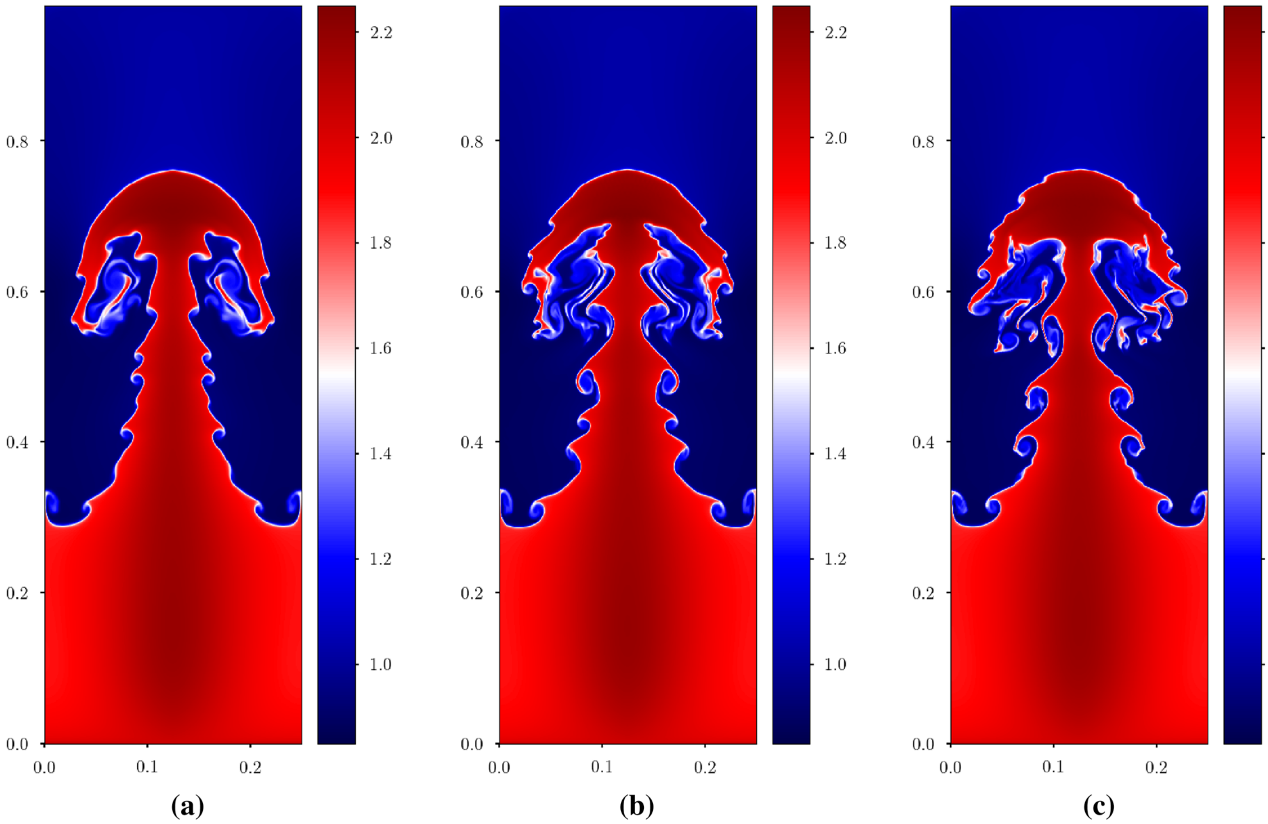

Fig. 9 Numerical solution for Rayleigh-Taylor instability test. Density contours are presented at $t = 1.95s$. CFL = 0.5. Grid 950×1000. **a** WENO-SV **b** WENO-Z+ and **c** WENO-SV

Fig. 10 The pressure vessel failed model is used as the onset of the physical explosion. The shock wave and associated discontinuities are resolved via the proposed WENO-SV scheme as sketched in the diagram above

applying WENO-SV. This behaviour is expected due to the similarity of the methods.

On the other hand, it is important to call attention that at this particular test case, we were concerned with the validation and verification of the new method proposed prior to applying it to the explosion problem.

Physical explosion modelling

It has been proposed the coupling of the WENO-SV scheme to deal with physical explosion in case of a (1) vessel rupture, named as PVF/WENO-SV model, and (2) blast waves through pipelines, named as WENO-SV/pipelines model.

Table 1 Thickness, tensible strength and radius of the Soda-lime glass sphere

Soda-lime glass characteristics	
Glass thickness (z)	0.89 m
Tensible strenght (S_{M1})	19 MPa
Tensible strenght (S_{M2})	41 MPa
Glass sphere radious (r_0)	0.051 m

Pressure vessel failed and WENO-SV model description

The main idea of the proposed model is as follows. Appropriate initial conditions for WENO-SV scheme are prescribed. The flowchart calculation procedure of the PVF/WENO-SV model is shown in Fig. 10. The Pressure Vessel Failed model (PVF model) (Crowl and Louvar 2002) is applied in order to set the initial condition for the vessel bursting pressure taking into account the dimensions, geometry and material of construction of the vessel. The WENO-SV scheme computes the flow of the shock wave over space and time.

The PVF model considers that the internal pressure required for the vessel rupture should be computed considering the pressure difference ($P - P_0$) and not exceeding 0.665 times the material mechanical strength (Crowl and Louvar 2002). It is evaluated as

$$P = P_0 + \frac{2S_M z}{r_0 + 0.2z} \tag{19}$$

or

$$P = P_0 + \frac{2S_M\left(\frac{z}{r_0}+1\right)^2 - 2S_M}{\left(\frac{z}{r_0}+1\right)^2 + 1} \tag{20}$$

for the exceeding cases. Here, we have P as the internal absolute pressure (Pa), P_0 is the atmospheric pressure (Pa), S_M is the tensile strength of the material (Pa), r_0 is the inside radius of the vessel (m), and z is the wall thickness of the vessel (m).

In order to validate the model, the physical explosion experiment performed by Boyer (1960) is used. The experiment Boyer (1960) considers the burst of a soda-lime glass sphere due to the increasing of the internal pressure. The features of the glass vesselsl are summarised in Table 1. The tensible strength (S_M) of the glass material was assumed to be within the range varying from 19 to 41 MPa ($S_{M1} = 19$ MPa and $S_{M2} = 41$ MPa). The pressure required for the soda-lime glass to rupture for the tensible strength (S_M) $S_{M1} = 19$ MPa and $S_{M2} = 41$ MPa was $P = 1.42$ MPa and $P = 2.95$ MPa, respectively.

The glass explosion took place in air at atmospheric pressure $P_0 = 0.1$ MPa and ambient temperature $T_0 = 25.85$ °C. The temperature inside the glass sphere was also $T = 25.85$ ° C.

WENO-SV/pipelines model description

The novel numerical scheme was also investigated in the scenario that the explosion took place inside a pipe. In this case, it has been considered the loss of energy due to the friction between the wall pipeline and the fluid flow.

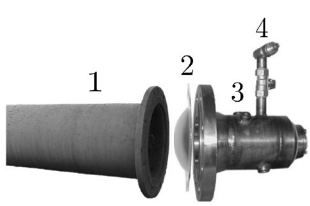

Fig. 11 Apparatus of the explosion experiment: (1) low pressure shock tube, (2) bursting membrane, (3) high pressure vessel, (4) solenoid valve. Adapted from Skacel et al. (2013)

For the pipeline model, the loss of energy was addressed by the modified Colebrook-White formulation as stated next

$$\begin{aligned} P_1^2 - P_2^2 &= \frac{q\,L\,s\,T\,Z}{176.85\,D^5}\frac{P_{st}^2}{T_{st}^2}\frac{1}{\mho}, \\ \mho &= -2log\left(\frac{\hat{\epsilon}}{3.7D} + \frac{2.825L}{Re\sqrt{f}}\right) \end{aligned} \tag{21}$$

where q is the volume gas flow rate, the length of the pipe is L, s is the relative density, T is the absolute temperature, Z is the gas compressibility factor, the diameter of the pipe is D. The standard pressure $P_{st} = 1.01325 \cdot 10^5$ Pa and the standard temperature $T_{st} = 288.15$ k. The friction factor, f', modelled by Colebrook-White formulation is defined below

$$\frac{1}{f'} = -2log\left(\frac{\hat{\epsilon}}{3.7D} + \frac{2.5L}{Re\sqrt{f'}}\right), \quad Re = \frac{\rho VD}{\mu} \tag{22}$$

where $\hat{\epsilon}$ is the material roughness, μ is the viscosity, ρ stands for the density and Re is the Reynolds number.

Skacel et al. (2013) conducted a physical explosion experiment considering a pipe connected to a vessel. The vessel was filled with nitrogen. As shown in Fig. 11, the apparatus consisted of a high pressure vessel (local of physical explosion) and a low pressure shock tube, both with diameter of 100 mm, separated by an aluminium membrane. The high pressure vessel achieved 700 kPa when the membrane broke up. The pressure wave travelled through the pipeline where measurements at different locations (1.21, 3.34, 5.84, 8.34 and 10.84 m) were taken.

Next section reproduces numerically both experiments described in the current section. The experiments have been used to validate the proposed numerical scheme based on the local Mach number.

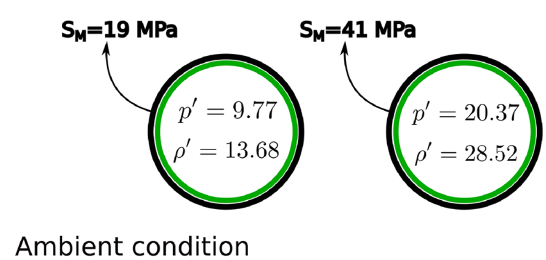

Fig. 12 Normalised density (ρ') and pressure (p') in the sphere. Tensile strength (S_M) of 19 MPa and 41 MPa have been considered. Normalised ambient density (ρ_0) and ambient pressure (p_0) are found outside the sphere

Results

This section addresses the numerical modelling of two experiments, namely bursting vessel and bursting pipeline. Although the experiments have been described in the previous section, details of the experiments considered here can be found elsewhere Boyer (1960) and Skacel et al. (2013), respectively.

Since we are interested in the performance of the novel WENO-SV scheme, we have used the bursting vessel and bursting pipeline experiment as the onset of the shock wave in order to verify how the numerical method copes with the discontinuity caused by the propagation of the shock wave.

Bursting vessel: PVF/WENO-SV model

The initial values used to perform the numerical simulation are calculated according to the tensible strength of the material used in Boyer (1960) experiment. The non-dimensionalised initial values are shown in Fig. 12 according to the material tensible strength considered.

Figure 13 shows the density contours at three instants of time. Analysis of Fig. 13a shows a significant difference in the density. At early stages it can be observed a region of high density close to the onset of the explosion followed by the density gradient. The second instant of time shows a pronounced region of high density (red). It can also be observed a sharp drop as highlighted in the second and third instant of time. Details of the variation of the density are shown in Fig. 13b. A second shock is clearly identified for all snapshots.

Figure 14 shows the pressure propagation. Analysis of Fig. 14 shows that pressure is hight in the centre of the explosion at early stages. As the time unfolds the pressure wave propagates leading to clear discontinuous regions shown by the second instant of the time from Fig. 14a. Figure 14b shows how the pressure varies as function of the radius. Analysis of the plot in Fig. 14b shows the propagation of the main shock and also the presence of the secondary shock.

Figures 13, 14 and 15 show the density, pressure and velocity waves profiles at nondimensional $t = 0.2$, $t = 0.3$ and $t = 0.4$, respectively. As the main shock propagates outwards, it becomes weaker. The density at the origin becomes lower than the density at the tail of the second shock wave. The velocity increases from zero at the head of the second shock to its tail and then it decreases. The contact discontinuity separates the expanded gas from the air compressed by the main shock. Figure 16 shows the density, pressure and velocity waves profiles at nondimensional $t = 0.6$, $t = 0.8$ and $t = 1.0$, respectively. The second shock starts reversing to the inward direction with increasing strength.

The wave profiles captured by WENO-SV scheme agree with those reported by Boyer (1960), Friedman (1961) and analysed theoretically by Brode (1957). The author in Brode (1957) solved the conservation equation by numerically integrating a set of stable approximate difference equations using a real-gas equation of state for air. It has incorporated the thermal and caloric equations for a non-real gas in the numerical solution of the point-source explosion in air. Figure 17 shows the comparison among the experimental data (Boyer 1960), analytical (Brode 1957) and numerical PVF/WENO-SV model calculation for the main shock wave. Also, the second shock and the discontinuity wave have been compared with the analytical data.

The qualitative comparison between experimental and numerical physical explosion of the glass sphere shows the high density region in the centre of explosion and a radial shock wave propagation through the low-pressure region, see Fig. 18.

Bursting pipeline: WENO-SV/pipelines model

In this section, the peak pressure is calculated using the developed method based on the coupling between high

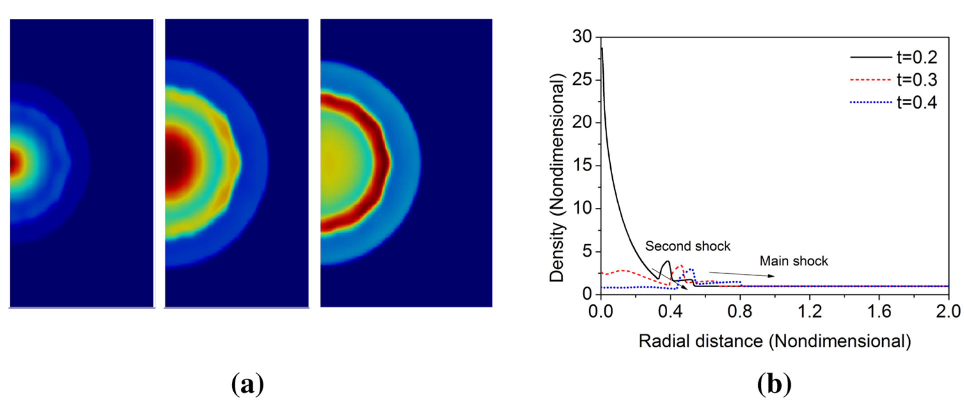

Fig. 13 Contours of normalised density at three instants of time, $t = 0.2$, $t = 0.3$ and $t = 0.4$ (**a**). Numerical findings of the normalised density at central line of shock wave (**b**)

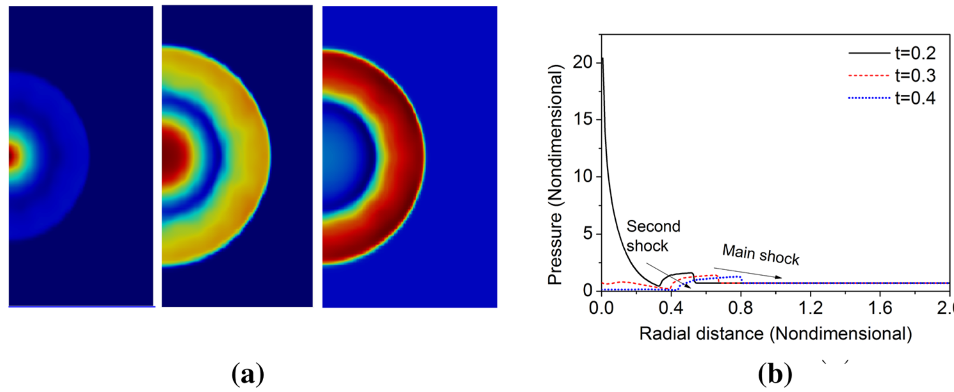

Fig. 14 Contours of normalised pressure at three instants of time, $t = 0.2$, $t = 0.3$ and $t = 0.4$ (**a**). Numerical findings of the normalised pressure at central line of shock wave (**b**)

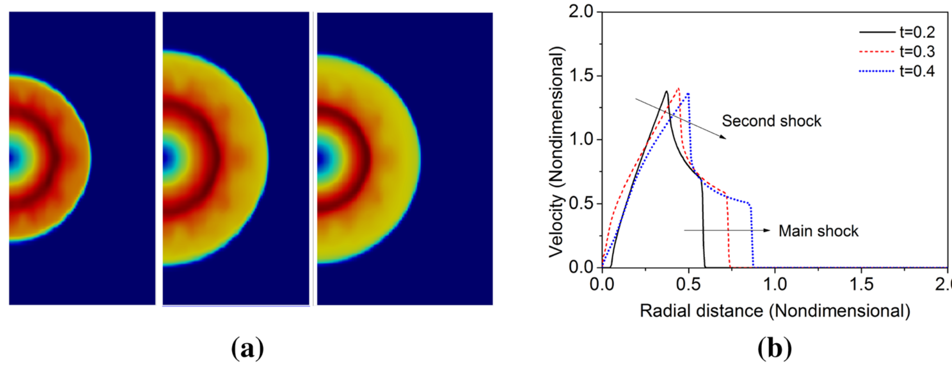

Fig. 15 Contours of normalised velocity at three instants of time, $t = 0.2$, $t = 0.3$ and $t = 0.4$ (**a**). Numerical findings of the normalised velocity at central line of shock wave (**b**)

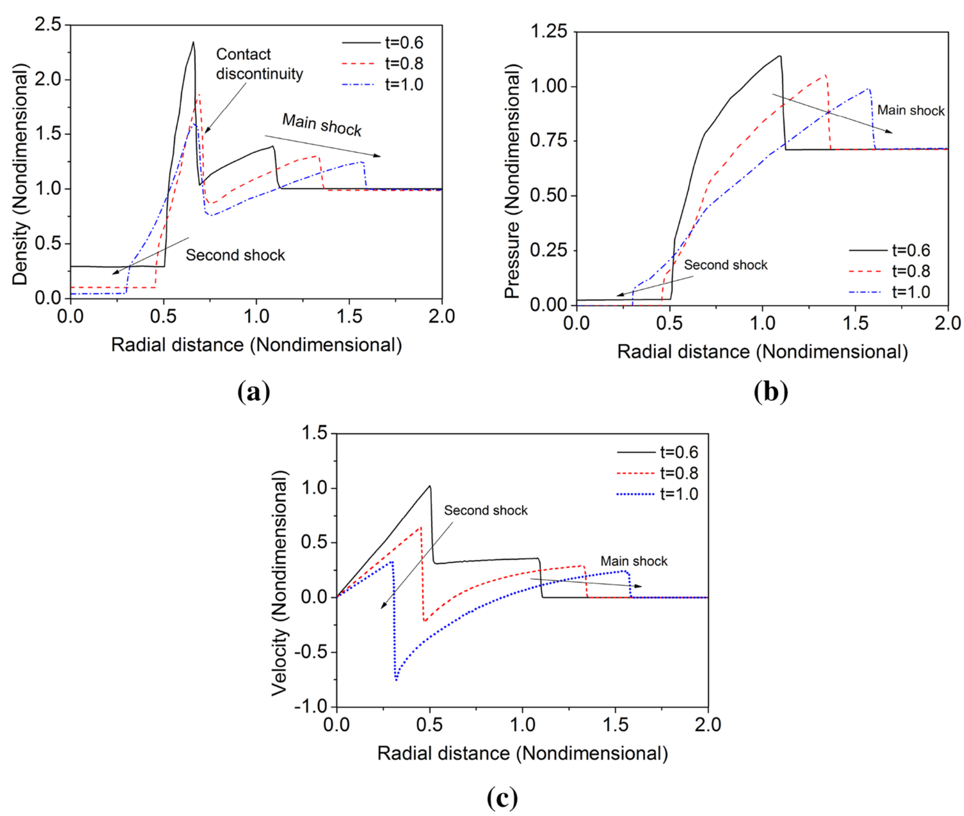

Fig. 16 Numerical simulation of physical explosion. Density, pressure and velocity profiles at different instants of time ($t = 0.6$, $t = 0.8$, $t = 1.0$)

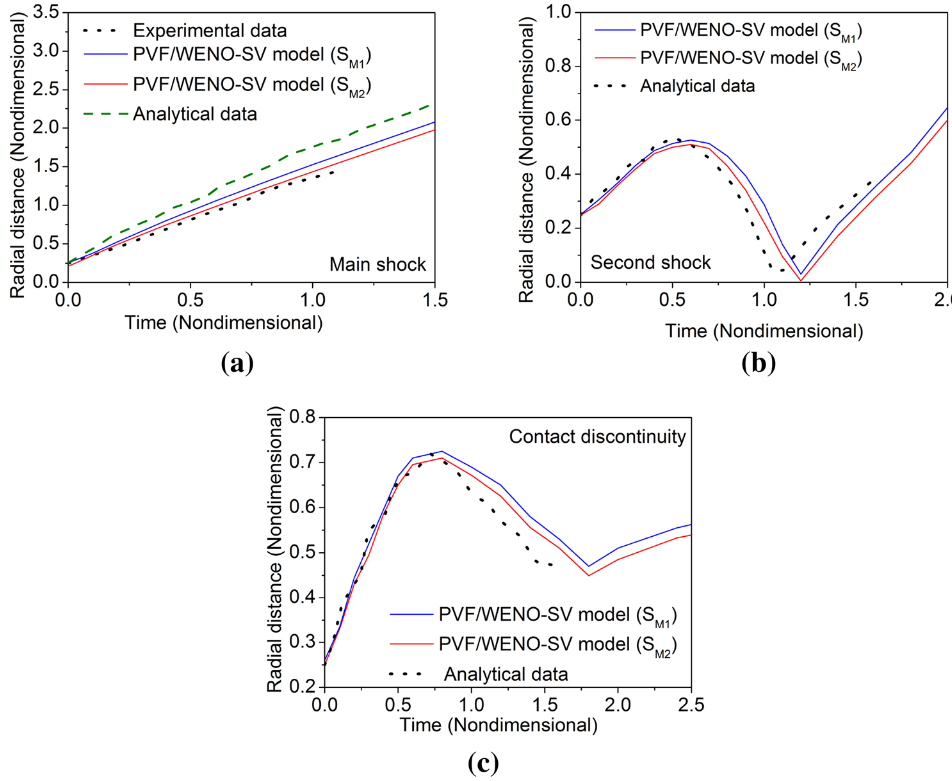

Fig. 17 Comparison among experimental data (Boyer 1960), analytical results (Boyer 1960) and PVF/WENO-SV findings for the main shock wave (a). The behaviour of the second shock. (b) Contact discontinuity and (c) the wave propagation

order WENO-SV scheme and MCW formulation previously described.

The numerical results are compared with the experimental data reported by Skacel et al. (2013). The pressure history is recorded at four positions in the pipe and it is shown in Fig. 19. Analysis of Fig. 19 shows the overpressure peak followed by the negative phase of the explosion. The arrival peak time is longer as the monitor point is placed further away from the onset of the explosion. The observed behaviour is in accordance with the current understanding of the explosion phenomena. This qualitative analysis emerges as an additional indication that the the proposed numerical method is able to capture the features of accidental explosion.

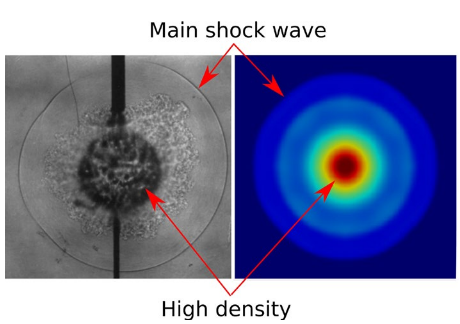

Fig. 18 Qualitative comparison between experimental physical explosion (Boyer 1960) and PVF/WENO-SV formulation

Figure 20 shows how the peak pressure decreases along the distance. Analysis of Fig. 20 shows that the sole implementation of WENO-SV scheme is not sufficient for capturing the full nature of the explosion in pipelines. On the other hand, the embedded modelling of the Modified Colebrook-White formulation led to very good agreement with experimental data.

Conclusions

We have proposed an enhanced numerical scheme for modelling of discontinuity in explosions. We have shown that by increasing the weight of less-smooth substencils led to less dissipative solution of the shock-entropy wave problem. The contribution from the less-smooth substencil was attained based on the local Mach number rather than the size of the mesh. In doing so, it was possible to take into account the underlying physics of the explosion problem. The challenges imposed by flows with high Mach numbers, where the influence of pressure at upstream events is constrained was addressed by modifying the λ parameter. Comparison with analytical solution and experimental data had provided evidence that the enhanced numerical method led to less dissipative solution and excellent agreement with experimental data.

Overall, the main shock wave and the second shock wave and regions of the discontinuities were well captured by

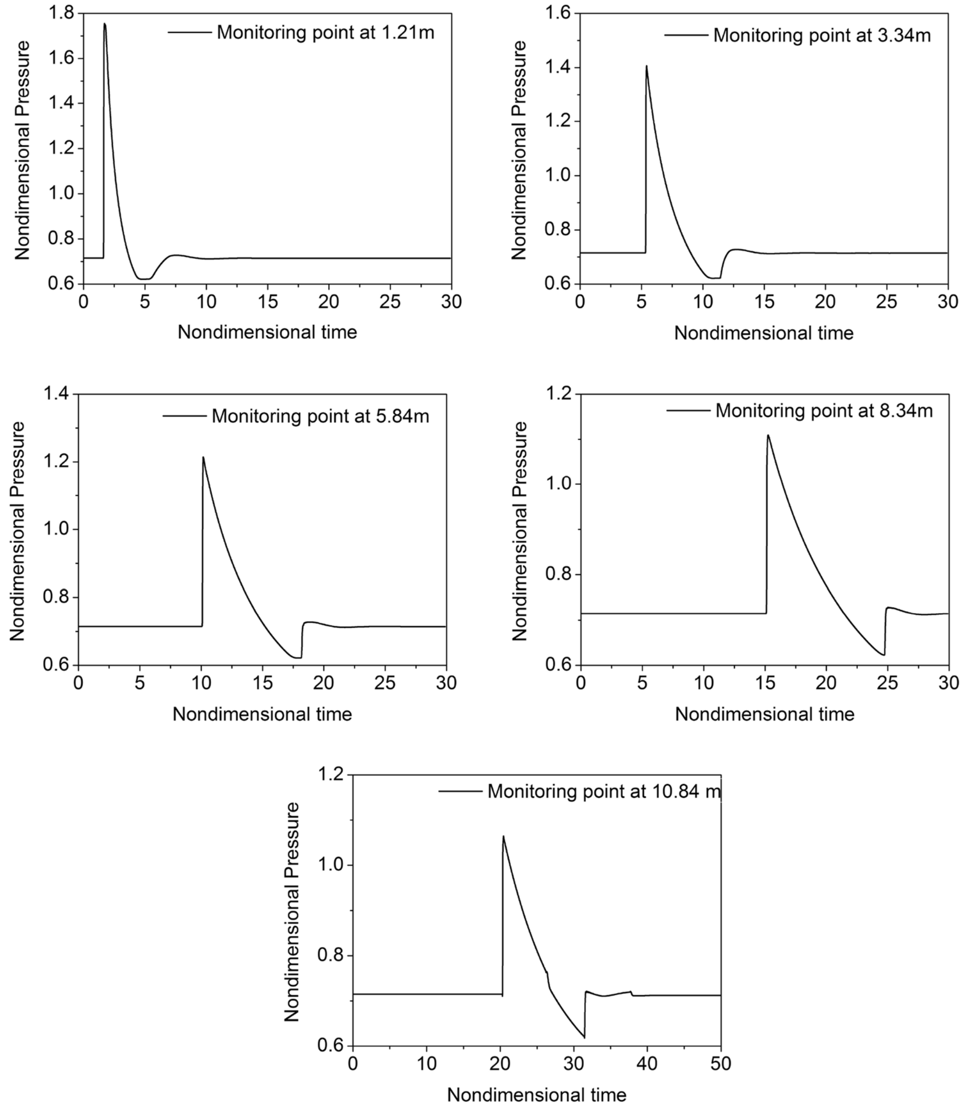

Fig. 19 Pressure history at the gauge position as reported in Skacel et al. (2013)

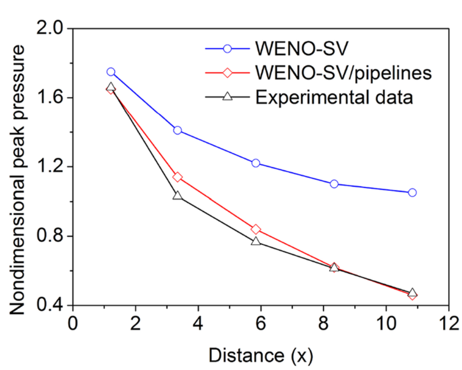

Fig. 20 Nondimensional peak pressure comparison among experimental data, WENO-SV and WENO-SV/pipelines

the proposed scheme. The main shock wave shows good agreement with experimental data and the second shock and discontinuities waves follow the same behaviour with good agreement when compared to analytical findings.

Furthermore, the proposed coupling PVF model and WENO-SV scheme emerge as an alternative computational tool to deal with an open field physical explosions from spherical vessels. The proposed coupling might be useful for consequence analysis and accidents investigation in the process industry. The pressure history was captured without spurious oscillations leading to good agreement.

Further investigation of the application of the proposed numerical scheme in other classes of physical problems is currently under investigation and it will be addressed in future publications.

Acknowledgements Thanks are due to CAPES grant number 33003017034-P8 for the financial support and CENAPAD-SP (National Centre for High Performance Computing in Sao Paulo, Brazil).

References

Abbasi T, Abbasi S (2007) J Hazard Mater 141(3):489. https://doi.org/10.1016/j.jhazmat.2006.09.056

Acker F, de R.Borges RB, Costa B (2016) J Comput Phys 313:726. https://doi.org/10.1016/j.jcp.2016.01.038

Borges R, Carmona M, Costa B, Don WS (2008) J Comput Phys 227(6):3191. https://doi.org/10.1016/j.jcp.2007.11.038

Boyer DW (1960) J Fluid Mech 9(3):401–429. https://doi.org/10.1017/S0022112060001195

Brode H (1957) Theoretical solutions of spherical shock tube blasts. The RAND Cor-poration, Santa Monica

Crowl DA, Louvar JF (2002) Chemical process safety. Fundamentals with applications. Prentice Hall, Upper Saddle River

De Rezende Borges RB (2017) ICOSAHOM 2016:547–559. https://doi.org/10.1007/978-3-319-65870-4_39

Ferreira ES Jr, Vianna SSV (2016) Braz J Chem Eng 33:525

Ferreira TD, Santos RG, Vianna SS (2019) Comput Methods Appl Mech Eng 352:417. https://doi.org/10.1016/j.cma.2019.04.023

Fi K (1999) J Hazard Mater 11:489–519

Fiates J, Vianna SS (2016) Process Saf Environ Prot 104:277. https://doi.org/10.1016/j.psep.2016.09.011

Friedman MP (1961) J Fluid Mech 11(1):1–15. https://doi.org/10.1017/S0022112061000810

Gottlieb S, Gottlieb D, Shu CW (2006) J Sci Comput 28(1):307–318. https://doi.org/10.1017/S0022112061000810

Hu F, Wang R, Chen X (2016) J Comput Appl Math 303:56. https://doi.org/10.1016/j.cam.2016.02.027

Jiang GS, Shu CW (1996) J Comput Phys 126(1):202. https://doi.org/10.1006/jcph.1996.0130

Khan FI, Abbasi S (1999) J Loss Prev Process Ind 12(5):361. https://doi.org/10.1016/S0950-4230(98)00062-X

Leak C (2002) A review of the state-of-the-art in gas explosion modelling. Health and Safety Laboratory, London

Lewis DJ (1980) Prog Energy Combust Sci 6(2):151. https://doi.org/10.1016/0360-1285(80)90004-0

Liu TG, Khoo BC, Yeo KS (1999) Int J Numer Methods Fluids 31:661–680

Oliveira RLF, Doubek G, Vianna SS (2019) Process Saf Environ Prot 123:358. https://doi.org/10.1016/j.psep.2018.12.031

Skacel R, Janovsky B, Dostal L, Svihovsky J (2013) J Loss Prev Process Ind 26(6):1590. https://doi.org/10.1016/j.jlp.2013.08.005

Wang C, Shu CW, Han W, Ning J (2013) Combust Flame 160(2):447. https://doi.org/10.1016/j.combustflame.2012.10.002

Wang C, Dong X, Shu CW (2015) J Comput Phys 298:161. https://doi.org/10.1016/j.jcp.2015.06.001

Xu W, Wu W, Lin Y (2018) Comput Math Appl 76(2):284. https://doi.org/10.1016/j.camwa.2018.04.019